ITER NBI operational window and power availability constraints due to shine-through losses

P. Vincenzi[1,2], M. Schneider[3], P. Veltri[3], J.F. Artaud[4], A. Loarte[3], S. Nicolici[3], C. Poggi[3], A.R. Polevoi[3], A. Snicker[5]

[1]Consorzio RFX, Padova, Italy
[2]Institute for Plasma Science and Technology, National Research Council, 35127 Padova, Italy
[3]ITER Organization, Route de Vinon-sur-Verdon, CS 90 046, 13067 St. Paul-lez-Durance, France
[4]CEA, IRFM, F-13108 Saint-Paul-lez-Durance, France
[5]VTT Technical Research Centre of Finland Ltd.

E-mail: pietro.vincenzi@igi.cnr.it

Abstract

This paper explores the operational boundaries and power availability of the neutral beam injection (NBI) system in ITER, with a specific focus on shine-through loss prevention. Shine-through, a phenomenon where part of the injected neutral beam remains un-ionized in the plasma and directly impacts the first wall components, poses a significant risk to the lifetime of ITER's plasma-facing components. The operational window for NBI is consequently constrained by these losses, which are influenced by factors such as plasma density, beam energy, and injection geometry. Leveraging advanced numerical simulations, we investigate these dependencies across various ITER plasma scenarios, particularly for the DT-1 phase, which will mark the first NBI operations. In light of recent ITER blanket design changes, our analysis refines previous estimates of the maximum acceptable shine-through power on plasma-facing components. We then present a new heuristic formula which permits the calculation of the shine-through fraction and the minimum plasma density that permits ITER NBI operations as a function of global variables. This allows for establishing operational limits for Hydrogen and Deuterium NBI in Hydrogen, Deuterium, and Deuterium-Tritium plasmas. Additionally, we compare commonly used beam ionisation codes for ITER and tokamak simulations, evaluating their reliability in the investigated parameter space. The findings of this study are crucial for ensuring the efficient operation of the NBI system during ITER's experimental phases. They define the conditions under which beam power can be fully utilised without compromising operational lifetime, thereby informing future plasma operation plans and contributing to the success of ITER's scientific objectives.

Keywords: ITER, NBI, shine-through, power load, auxiliary power, H&CD

1. Introduction and motivation

As the construction of ITER progresses, its research plan, detailed initially in **[1]**, has undergone a recent review **[2]**, **[3]**. This update aims to align the plan with the current construction timeline while accelerating and securing the path toward the nuclear phase. Operations will be conducted at half and full toroidal magnetic field (B_t = 2.65 / 5.3 T at major radius R = 6.2 m). They will focus exclusively on Hydrogen (H), Deuterium (D), and Deuterium-Tritium (D-T) plasmas. ITER will begin operations with reactor-relevant, full Tungsten plasma-facing components (PFCs), replacing the originally planned Beryllium wall. The heating and current drive (H&CD) power mix has also been adjusted. After the "Start of Research Operation" (SRO) phase, which relies on wave heating, the second phase ("DT-1") will see the use of two neutral beam (NB) injectors delivering up to 33 MW of power in total. In the later third phase ("DT-2"), a third NB injector can be installed to increase the available auxiliary power. The ITER goal in DT-1 is to reach D-T operation with high fusion gain $Q = P_{fusion}/P_{H\&CD} \geq 10$. High fusion gain requires operation in plasma high-confinement mode regime (H-mode) **[4]**. H-mode access, which will be first tested in H and D plasmas, requires full H&CD power availability, which is critical for ITER's success. Under specific conditions, ITER's high-energy neutral beams (with particle energy up to E_{NBI} = 1 MeV for D injection) may not ionise sufficiently, leading to the so-called shine-through (ST) losses, where beam power is deposited on PFCs. These losses are influenced by factors such as injection energy, beam species, and plasma properties, particularly plasma kinetic profiles and composition **[5]**. Monitoring shine-through is essential, as excessive loads can cause the degradation of the PFCs. While machine lifetime must be ensured, maximising NB injector performance is crucial to achieving ITER's scientific goals. Besides shine-through, other resonant phenomena can determine localised energetic particle losses **[6]**, like toroidal magnetic field ripple, which is well mitigated by ferromagnetic inserts **[7]**. Other losses, such as those due to Alfvenic eigenmodes, can also be managed **[8]** with the specific beam injection geometry considered for the present work (as reported in **[6]**). In **[6]**, the minimum plasma density required to prevent harmful shine-through was estimated for previous ITER research scenarios, and work in **[9]** extended the investigated parameter space in the previously foreseen H and He plasmas. In this paper, we focus on the updated DT-1 phase H, D and D-T plasmas, refining the calculation of the beam footprint on the recently modified plasma-facing components to estimate the maximum allowable shine-through power load. We further expand the analysis of ITER shine-through dependences using advanced numerical simulations, investigating off- and on-axis beam injection geometries. These findings finally define the unrestricted operational space for ITER Neutral Beam Injection (NBI) and the power available for various scenarios. Additionally, this paper compares different beam ionisation codes, discussing the reliability of predictions and potential limitations in specific simulation conditions.

2. ITER NBI geometry and shine-through power load limits with the new blanket design

Starting from the DT-1 operation phase, ITER foresees the operation of two heating neutral beam injectors **[10]** with a similar range of tuneable parameters, each providing 16.5 MW of power to the plasma through 1280 beamlets per beamline. NBI operations will start in H plasmas, then D and last D-T. To allow beam power deposition in the plasma's core, ITER NB injectors will accelerate D particles to energy up to E_{NBI} = 1 MeV (or up to 870 keV for H injection). This injection energy requires the acceleration of negative ions from the beam source, and specific R&D is ongoing to successfully build and operate an ITER NB injector prototype **[11]**, **[12]**. In ITER NBI, an injection energy reduction is possible until 500 keV but only accompanied by a power reduction ($P_{NBI} \sim E_{NBI}^{2.5}$). This is necessary to maintain the beam perveance that keeps the beam optical properties within the design specification, i.e. to avoid the beam's excessive widening at lower injection energy. The beams are injected tangentially into the plasma (with a tangency radius of $R_{tang} \sim 5.3$ m), and they point downwards with their axis inclined vertically of -49.2 mrad. This injection geometry allows to drive non-inductive currents and uniquely provides toroidal momentum to the plasma **[6]**. ITER beams can be vertically tilted during operations within a range of ± 10 mrad with respect to their nominal axis. In particular, they can be injected in an almost on- (+10 mrad) or off-axis (-10 mrad) geometry to affect NB current drive and to have the control of beam particle and energy deposition to prevent the excitation of Alfvenic eigenmodes **[8]**. ITER off/on NB injection geometry is pictured in Fig. 1.

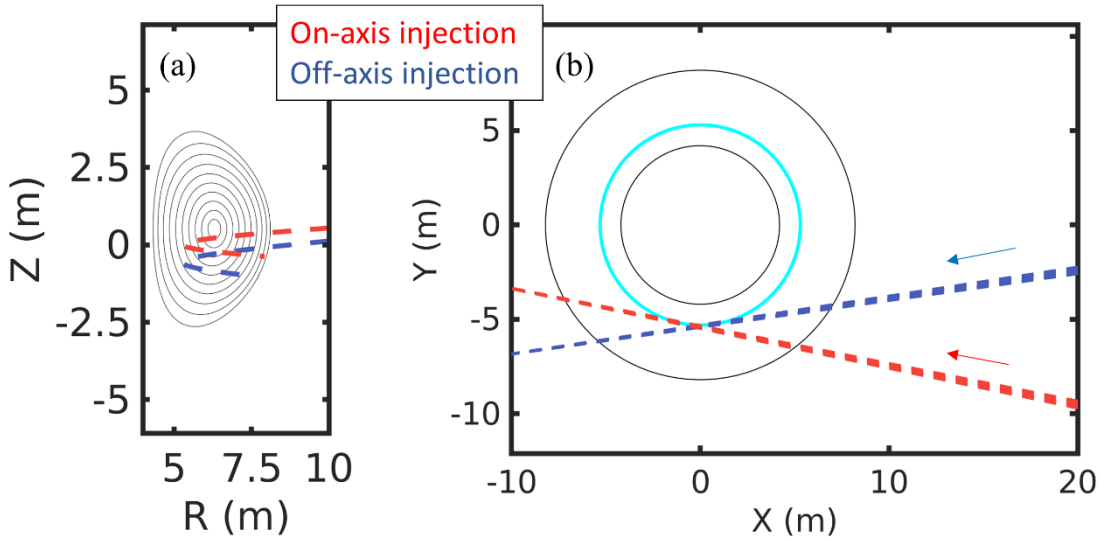

Figure 1: ITER neutral beam injection geometry in configuration "off/on" with one injector in the off-axis vertical tilt configuration (blue) and one in the on-axis configuration (red). (a) shows a poloidal projection, while (b) a view from above the torus, with the circumference of radius R_{tang} represented in cyan.

The evaluation of the maximum acceptable shine-through fraction on the surface of the ITER blanket is based on the power loading calculated with the BTR code **[13]** and considers the latest design of the blanket. In BTR, the particles carried by each of the 1280 individual beamlets composing the full beam are sampled with a high number of discrete macro-particles representing each a large ensemble of neutral particles, according to a bi-gaussian angular distribution **[14]**. The latter accounts for the beamlet divergence, aiming angle, and possible misalignments. The macro-particles are traced from the exit of the accelerator, all along the NBI beamline and inside the ITER volume. The power density of the beam can be obtained on an arbitrary surface intersecting the beam path. In our simulations, we calculated the projection of the NBI power footprint on the surfaces normal to the realistic plasma-facing elements in the NBI wetted area, which can be seen in Fig. 2. Regarding the beam tilting, two cases were considered: the first corresponded to a beam travelling along the NB axis (i.e. with an angle of -49.2 mrad and zero mrad of source tilting) and another injected with a source tilting of +10 mrad, upward (the so-called "on-axis" injection geometry). In both cases, the nominal power of 16.5 MW was used, and a beamlet divergence of 5 mrad. Without the plasma, i.e. the beam fired in vacuum, the maximum projected power density on the PFCs associated with both cases is ~ 40 MW/m^2. The maximum NBI power density acceptable on the PFCs is about 4.4 MW/m^2 **[6]** (obtained from the PFC power density limit of 4.7 MW/m^2 - given by the PFC armour bond and critical heat flux limits - subtracted by the amount due to plasma radiation and charge exchange loads, assumed as 0.3 MW/m^2 **[15]**). These numbers suggest a maximum allowed shine-through fraction of about 11% when firing the beam at maximum power. A power limit of 10% shine-through is used in the following to account for possible additional loads due to convective plasma heat fluxes; this is considered a conservative assumption. As already observed in **[6]**, the shine-through limit shall also consider the fact that a fraction of the beam will penetrate the 10mm wide poloidal horizontal gap (see the horizontal gap in Fig. 2a) between the two sets of PFC modules reaching the blanket shield block 16S behind them (the wetted area of Fig. 2b). The associated power density depends on the beam tilting angle. It is maximum for the case of 0 mrad tilting, for which the beam axis intercepts exactly the horizontal gap, with a power density reaching a localised peak of 5.5 MW/m^2. The average power density acceptable on the shield block is about 0.35 MW/m^2, but higher values can be tolerated locally. For the power distribution calculated for the 0 mrad case, it is estimated that the acceptable shine-through fraction is about 8% **[16]**, which is, therefore, more restrictive than the limit imposed by the PFC constraints. For the case of +10 mrad tilting angle (and, for symmetry reasons, -10 mrad), the peak of power is moved away from the gap so that the maximum acceptable shine-trough fraction increases up to 10% at the maximum beam power, in line with the limit imposed by the first wall. These numbers are a factor of 2 higher than the limits obtained in **[6]** and reflect the successful re-design of the blanket.

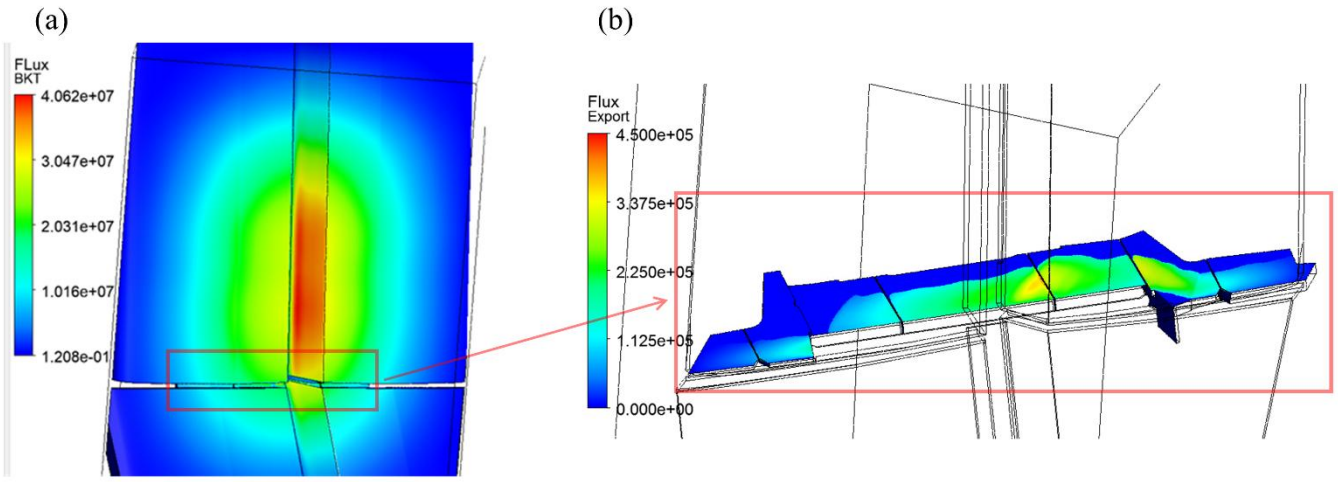

Figure 2: Power density on the blanket modules (MW/m²) for the on-axis injection case (+10 mrad vertical tilt) is shown in (a). Panel (b) provides a close-up view, highlighting the power density passing through the gap between blanket modules (visible in (a)) and impacting the shield block area exposed to the beam.

3. Numerical simulations of ITER NBI shine-through

ITER NB injection (NBI) shine-through (ST) is studied in the present work through a wide-range parameter scan using state-of-the-art numerical simulations. The Integrated Modelling and Analysis Suite (IMAS) **[17]** is the numerical framework used to interface the different codes to complete our task, as tested with a similar scheme in **[9]**. The workflow developed consists of a simplified 0.5D plasma transport solver (METIS **[18]**), a fixed-boundary magnetic equilibrium solver (CHEASE **[19]**), and an NB ionisation code. In METIS, the density profiles are evolved from prescribed line-averaged density, using scaling laws for peaking and edge density. The evolution of the 0D plasma energy content is calculated using an ODE solver based on scaling laws. The 1D temperature profiles are calculated from stationary heat transport equations using transport coefficients scaled on the plasma energy content for their time evolution. CHEASE equilibrium code is then used to refine the METIS magnetic equilibrium calculated with a 3-moment description, before using the NB ionisation code. We used both NEMO **[20]** and BBNBI **[21]** IMAS actors for this last step. NEMO code uses a "narrow beam" model approximation for each beam source. In contrast, the BBNBI Monte Carlo code simulates the beam trajectory and ionisation considering test particles generated from each single beamlet. BBNBI IMAS actor uses Suzuki ionisation cross sections **[5]**, while NEMO uses ADAS cross sections **[22]**. Both codes consider the multi-step ionisation process from excited plasma ions, which is relevant at high injection energies as in the ITER case. Ionisation cross sections in the high energy range of ITER injection are derived theoretically; therefore, their validity will be, at least partly, addressed in the first JT-60SA plasma operations with 500 keV, planned to happen in the near future **[23]**. To account for all DT-1 phase plasmas, we have simulated five cases: H plasmas with H NBI, D plasmas with D or H NBI and D-T plasmas with D or H NBI. We identified the parameters for our scan by considering the main dependences of beam shine-through: plasma density and beam injection energy E_{NBI}. In particular, not only the plasma line averaged electron density $n_{e,line}$ has been considered, but also the so-called density-peaking factor, i.e. the ratio of the central electron density to the volume-averaged electron density, $n_{pf} = n_{e,0}/\langle n_e \rangle$. The density-peaking factor is a parameter that describes the profile "shape", and it indeed affects beam shine-through since it is related to the density that is actually seen by beam particles on their path through the plasma (see, e.g. Fig. 6 of **[9]**). However, the density-peaking factor has not been considered thoroughly in previous work as a free parameter **[6]** when defining the ITER NBI operational space for the former ITER research plan and blanket design. Other parameters are known to affect beam ionisation cross-section, albeit to a lesser extent, such as plasma electron temperature and impurity content; dependencies on these parameters are discussed later in this section.

The plasma density, its peaking factor and beam injection energy (with injected power varying as $P_{NBI} \sim E_{NBI}^{2.5}$) are varied in METIS plasma simulations as in Table 1 to build an IMAS plasma database. Plasma density has been varied to account for the range of plasma operations foreseen **[3]**, considering that shine-through losses are relevant at low density, while they become rapidly negligible at larger densities. The peaking factor varies from a completely flat density profile ($n_{pf} = 1$) to a peaked one ($n_{pf} = 1.5$), considering that $n_{pf} = 1.2$ is used for reference METIS H-mode scenarios modelling studies to represent the expected density profile peaking of ITER plasmas **[3]**. Finally, the injection energy is limited by injector capabilities described in Sec. 2. METIS simulations consider two impurities, which are set to be W to account for wall impurities and Ne as the radiative

impurity. The concentration of these impurities has been set to result in a plasma effective charge Z_{eff} of 1.2; this value has also been scanned, and shine-through results with different impurity concentrations are shown later in this section. BBNBI and NEMO both simulate the injection from the two NB systems with an injection geometry configuration called "off/on", i.e. one injector in the off-axis geometry (-10 mrad of vertical tilt) and one in the on-axis geometry (+10 mrad), as represented in Fig. 1. Off/on configuration in our simulations allows the independent estimation of beam shine-through for both the most convenient beam injection geometries in terms of minimisation of beam particle losses **[6]**. For each of the five plasma/NBI species cases, 288 cases have been run (8 $n_{e,line}$ × 6 n_{pf} × 6 E_{NBI} cases as listed in Table 1).

Line averaged electron density $n_{e,line}$ [10^{19} m^{-3}]		*Electron density-peaking factor $n_{pf} = n_{e,0}/\langle n_e \rangle$*		*Injected NB particle energy (E_{NBI}) and total power (P_{NBI})*		
#	**H, D, D-T plasmas**	**#**	**H, D, D-T plasmas**	**#**	**H NBI**	**D NBI**
n1	0.60	*npf1*	1.0	*E1*	500 keV, 8.26 MW	500 keV, 5.83 MW
n2	1.24	*npf2*	1.1	*E2*	574 keV, 11.67 MW	600 keV, 9.20 MW
n3	1,88	*npf3*	1.2	*E3*	648 keV, 15.80 MW	700 keV, 13.53 MW
n4	2.52	*npf4*	1.3	*E4*	722 keV, 20.70 MW	800 keV, 18.89 MW
n5	3.15	*npf5*	1.4	*E5*	796 keV, 26.42 MW	900 keV, 25.36 MW
n6	3.79	*npf6*	1.5	*E6*	870 keV, 33.00 MW	1000 keV, 33.00 MW
n7	4.43					
n8	5.07					

Table 1: Plasma and NBI parameters varied in numerical simulations to assess ITER NBI shine-through.

Using a similar method as in **[24]**, **[25]**, **[9]** and **[26]**, we have retrieved a heuristic formula to describe ITER NBI shine-through fraction dependencies. We assumed an exponential dependence of the shine-through fraction on the considered parameters ($n_{e,line}$ [10^{19} m^{-3}], n_{pf}, E_{NBI} [keV]) and performed a multi-linear regression on the twice logarithm of:

$$ST_{fraction} = exp\left(-\frac{{n_{e,line}}^{\alpha}\, {n_{pf}}^{\beta}\, {E_{NBI}}^{\gamma}}{\delta}\right) \quad (1)$$

where α, β, γ and δ represent the degrees of freedom of the regression, estimated by a least square method. A comparison of NEMO and BBNBI shine-through results is reported in Sec. 5, and due to the excellent agreement between the codes, we averaged NEMO and BBNBI results for our regression. To avoid unconverging Monte Carlo simulations, BBNBI has been programmed to interrupt the simulation when the ST is larger than 0.5; only NEMO results are used in those cases. Large ST fraction simulation cases do not represent planned ITER operations since machine protection systems will prevent NBI operations with ST larger than ~ 0.1, as detailed in Sec. 2. Table 2 reports the regression coefficients for each plasma/NBI species case. We performed a separate regression for off-axis injection, on-axis injection, and the average results of the two injection geometries.

Case 1	**H plasma, H NBI**		
	On/off-axis average	**Off-axis NBI**	**On-axis NBI**
RMSE	4.93 %	5.20 %	5.45 %
α	1.196 ± 4.05e-07	1.198 ± 4.28e-07	1.196 ± 4.04e-07

β	0.156 ± 9.67e-06	0.097 ± 1.02e-05	0.217 ± 9.65e-06
γ	-0.835 ± 5.19e-06	-0.835 ± 5.49e-06	-0.835 ± 5.18e-06
δ	8.41e-03 ± 1.86e-06	8.43e-03 ± 1.97e-06	8.33e-03 ± 1.84e-06

Case 2	**D plasma, H NBI**		
	On/off-axis average	**Off-axis NBI**	**On-axis NBI**
RMSE	2.46 %	2.66 %	3.29 %
α	1.152 ± 1.07e-07	1.153 ± 1.15e-07	1.152 ± 1.23e-07
β	0.172 ± 2.56e-06	0.118 ± 2.75e-06	0.228 ± 2.94e-06
γ	-0.781 ± 1.38e-06	-0.783 ± 1.48e-06	-0.780 ± 1.58e-06
δ	1.22e-02 ± 7.13e-07	1.21e-02 ± 7.61e-07	1.22e-02 ± 8.18e-07

Case 3	**D plasma, D NBI**		
	On/off-axis average	**Off-axis NBI**	**On-axis NBI**
RMSE	4.72 %	6.78 %	7.04 %
α	1.168 ± 9.38e-08	1.170 ± 1.26e-07	1.167 ± 1.18e-07
β	0.169 ± 1.05e-06	0.104 ± 1.42e-06	0.240 ± 1.32e-06
γ	-0.734 ± 3.62e-07	-0.741 ± 4.86e-07	-0.730 ± 4.54e-07
δ	1.02e-02 ± 1.62e-07	9.77e-03 ± 2.09e-07	1.04e-02 ± 2.08e-07

Case 4	**D-T plasma, H NBI**		
	On/off-axis average	**Off-axis NBI**	**On-axis NBI**
RMSE	2.69 %	2.94 %	3.44 %
α	1.134 ± 1.22e-07	1.135 ± 1.39e-07	1.132 ± 1.37e-07
β	0.178 ± 2.92e-06	0.121 ± 3.31e-06	0.237 ± 3.28e-06
γ	-0.771 ± 1.57e-06	-0.775 ± 1.78e-06	-0.767 ± 1.76e-06
δ	1.28e-02 ± 8.57e-07	1.26e-02 ± 9.51e-07	1.31e-02 ± 9.78e-07

Case 5	**D-T plasma, D NBI**		
	On/off-axis average	**Off-axis NBI**	**On-axis NBI**
RMSE	4.82 %	6.22 %	7.69 %
α	1.134 ± 1.03e-07	1.137 ± 1.34e-07	1.133 ± 1.30e-07
β	0.172 ± 1.57e-06	0.118 ± 1.51e-06	0.231 ± 1.46e-06
γ	-0.708 ± 3.97e-07	-0.713 ± 5.18e-07	-0.705 ± 5.02e-07
δ	1.17e-02 ± 2.04e-07	1.14e-02 ± 2.59e-07	1.19e-02 ± 2.62e-07

Table 2: Regression parameters for the shine-through fraction formula in eq. 1 for ITER DT-1 phase plasmas in off-axis, on-axis, and off-/on-axis averaged injection geometries.

Looking at regression results and the Root Mean Squared Error (RMSE) of the various cases in Tab. 2, eq. 1 describes the trends of the numerical simulations well. Interestingly, the injection geometry effect is well captured by the density-peaking factor parameter: by changing the injection geometry from off- to on-axis, a clear variation is seen only in β, while the other coefficients stay almost constant. If a density-peaking factor > 1 is present, the off-axis beam encounters lower density on its way through the plasma with respect to the on-axis beam. The geometrical injection effect is evident in Fig. 3a, which shows lower ST for the on-axis injection line at the same scan parameters. Increasing the density-peaking factor causes the ST to decrease since both injection lines cross the core, density-peaked region, to some extent. The dependence of ST on injection energy (γ coefficient in Tab. 2) is stronger when changing the injected species than when changing the plasma species. In contrast, the ST dependence on line-averaged density (α coefficient in Tab. 2) is stronger when changing the plasma species than the beam-injected species.

The injection of H beams has the cost of almost doubling the ST compared to D NB injection in the same plasma and at the same injection energy. This can be seen in Fig. 3b, especially in the low ST fraction range, which is of interest to ITER, where D injection generates about half or even less of the ST with respect to H beams for the same $n_{e,line}$, n_{pf} and E_{NBI}. As the discussion pertains to ST fractions, the different available beam power characterising the injection of H and D beams at the same energy (see Tab. 1) does not play a role here.

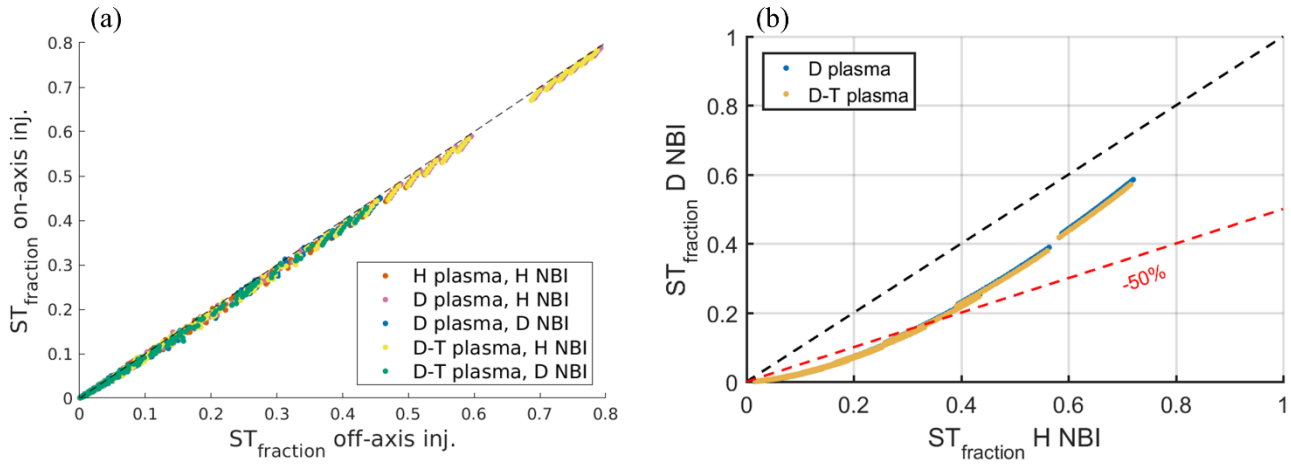

Figure 3: (a) compares shine-through loss fraction with off- and on-axis injection geometry. (b) shows a comparison of shine-through loss fraction when injecting D NBI versus H NBI in the same D or D-T plasmas.

At beam injection energies in the ITER range, the ionisation cross-section due to the energetic particle's impact with electrons becomes comparable to the one due to the ionisation by plasma ions at low plasma electron temperatures ($T_e \sim 1$ keV), while it decreases at larger electron temperatures. The total ionisation cross-section, i.e. the sum of all ionisation processes, has, therefore, a weak dependence on electron temperature. In our database, plasmas are self-consistently simulated with METIS; thus, there is a strong correlation between the electron temperature and the density given by the plasma transport regime. On the other hand, we wanted to understand the effect of electron temperature on ST in ITER plasmas. To disentangle the n_e-T_e correlation, we produced an ITER D plasma simulation and set the injected NBI power to zero. We then arbitrarily increased the ECRH input power at constant plasma density and profile shape to affect only the electron temperature. We obtained 21 plasmas with different electron temperatures at the same plasma density, with a mean volume-averaged temperature of the set of $T_{e,vol} = 17.23$ keV ± 5.54, ranging from $T_{e,vol} = 2.46$ keV to $T_{e,vol} = 23.68$ keV, well representing the foreseen ITER D plasmas. BBNBI and NEMO were then run to estimate beam ST on these plasmas. Results are shown in Fig. 4a.

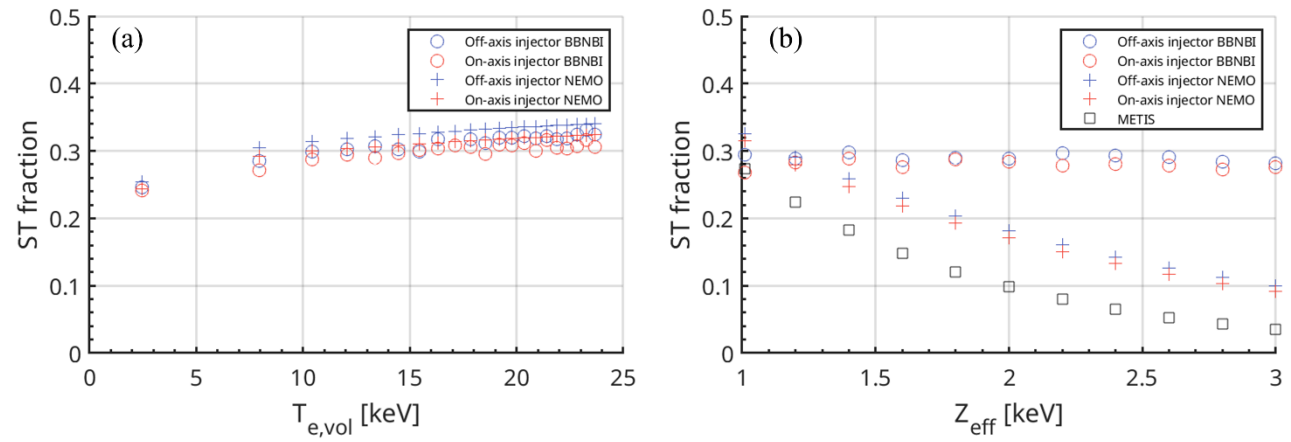

Figure 4. Dependence of shine-through loss fraction on the volume averaged electron temperature $T_{e,vol}$ in a D plasma for both injection lines, as calculated by BBNBI and NEMO codes (a). (b) reports the dependence of shine-through loss fraction on the plasma effective charge Z_{eff} in a D plasma, as estimated by BBNBI, NEMO and METIS.

As a general trend, we can see an increase in beam ST with $T_{e,vol}$, as expected. This increase is more significant in the low $T_{e,vol}$ range (< 10 keV), while the ST fraction only slightly increases by about 5% when passing from $T_{e,vol} = 10$ keV to ~ 25 keV. NEMO predicts a larger ST than BBNBI, and this difference is due to ADAS versus Suzuki ionisation cross-sections. Running NEMO with the outdated Janev ionisation cross sections **[27]** (a possible option of the code) resulted in better agreement with BBNBI due to Suzuki's model similarity with respect to Janev's.

Plasma impurities are also known to affect NB ionisation. Similarly to the previous scan, we prepared 11 identical METIS plasmas but changed the effective charge Z_{eff} from 1 to 3 (the reference value for ITER scenarios used in this paper is Z_{eff} =

1.2). In our METIS simulations, Z_{eff} profile is assumed flat. The ST fraction results from BBNBI and NEMO are shown in Fig. 4b. We can see that NEMO captures the impurity effect as expected from the ionisation cross-section dependence **[5]**, with a reduction of ST in the case of larger impurity content. However, BBNBI does not correctly mimic the impurity effect when increasing Z_{eff}. This issue is currently being addressed, and it is likely related to the correct input reading in the IMAS environment. However, it does not affect our main study performed at the reference Z_{eff} value of 1.2 since BBNBI and NEMO agree perfectly for Z_{eff} = 1.2. In Fig. 4b, we also added METIS ST fraction estimation. Differently from the $T_{e,vol}$ scan, in this Z_{eff} scan, METIS has been run including NBI, and METIS can estimate the ST fraction with an analytical model that exploits a beam attenuation equation and Suzuki ionisation cross-sections **[5]**. METIS describes the two NB injectors in a simplified way (see, e.g. the detailed explanation in **[25]**), which cannot be compared to the accuracy of NEMO and BBNBI codes. For these reasons, we averaged the METIS ST fraction over the two injection lines, and we did not expect a perfect match of METIS ST results with the other codes. However, it resulted in METIS including the Z_{eff} effect with the correct trend. Sec. 5 of this paper reports deeper discussions on code comparisons. In general, the effective charge as a global variable is not perfect. The stopping cross section depends on the mix of species in both models **[5]** (used in BBNBI) and **[27]**, which consider different sets of impurity species. Thus, it is possible to expect better agreement between code prediction for lower NBI energies where the role of excitation in the ionisation processes is less relevant and the importance of the charge-exchange processes with thermal ions increases.

4. Minimum plasma density and power availability for NBI operations

Due to beam perveance constraints, the ITER NB power from a single injector depends on the injection energy as:

$$\boldsymbol{P_{NBI}[MW] = 16.5\left(\frac{E_{NBI}}{E_{NBI,max}}\right)^{2.5}} \qquad (2)$$

with the maximum beam energy $\boldsymbol{E_{NBI,max}}$ being 870 keV and 1 MeV, respectively for H and D injection. The ST power arriving at the ITER PFCs is then:

$$\boldsymbol{ST_{power}[MW] = P_{NBI} \cdot ST_{fraction}} \qquad (3)$$

with $ST_{fraction}$ as defined in eq. 1. In Sec. 2, we discussed the ST limit for unrestricted ITER operations, which resulted in 10% and 8% of the maximum NB injected power, respectively, for fully vertically tilted beamlines and no vertically tilted lines, independently of the injected species. Our work uses the vertically tilted option since it is the optimal solution to minimise fast particle losses **[6]**. We assume an identical ST power limit of 10% for both off- and on-axis geometry for symmetry reasons since the beam shape can be well approximated by a Gaussian (as in **[6]**), with the beam axis impinging in the gap between identical blanket modules. Therefore, the ST power limit is 10% of 16.5 MW per injection line, i.e., 1.65 MW of power deposited to the PFCs. Considering this limit, we now calculate the minimum line-averaged plasma electron density that permits the operation of the ITER NB systems. From eq. 3, imposing ST_{power} = 1.65, we can derive:

$$\boldsymbol{n_{e,line,min} = \left(\frac{-ln\left(\frac{0.1}{(E_{NBI}/E_{NBI,max})^{2.5}}\right)}{n_{pf}^{\beta}\, E_{NBI}^{\gamma}}\,\delta\right)^{\frac{1}{\alpha}}} \qquad (4)$$

$n_{e,line,min}$ (in 10^{19} m^{-3}) in eq. 4 depends on the beam injection energy (keV) and the electron density-peaking factor (n_{pf}). Fig. 5a shows $n_{e,line,min}$ as a function of beam energy for three different n_{pf} values for a fully vertically tilted H and D (on-axis) injection in a D plasma. It is possible to see that $n_{e,line,min}$ strongly depend on the injection energy and injection species, with D injection having a significantly lower density limit. The density-peaking factor has a smaller effect, which becomes more evident when the injection energy increases. Tab. 3 reports the density limit $n_{e,line,min}$ for ITER NBI operations. Previous studies **[6]** reported a $n_{e,line,min}$ of $4.4 \cdot 10^{19}$ m^{-3} for H NBI in H plasma and $2.2 \cdot 10^{19}$ m^{-3} for D NBI in D plasma, though with different model assumptions, former power load limit on the blanket and without specifying the density-peaking factor which we demonstrated to play a role.

$\boldsymbol{n_{e,line,min}}$ **[10^{19} m^{-3}]**	**H NBI (E_{NBI} = 870 keV, $P_{NBI,tot}$ = 33 MW)**			**D NBI (E_{NBI} = 1 MeV, $P_{NBI,tot}$ = 33 MW)**		
	n_{pf} = 1 (flat denisty profile)	n_{pf} = 1.2	n_{pf} = 1.5 (peaked density profile)	n_{pf} = 1 (flat denisty profile)	n_{pf} = 1.2	n_{pf} = 1.5 (peaked density profile)
H plasma	4.14	4.01	3.85			

D plasma	4.39	4.24	4.05	3.08	2.97	2.83
D-T plasma	4.44	4.27	4.08	3.06	2.95	2.82

Due to density and injection energy dependence of eq. 1, $n_{e,line,min}$ depends almost linearly on the injection energy, as seen in Fig. 5a. We can approximate the maximum allowed injection energy to operate ITER NB systems as:

$$\boldsymbol{E_{NBI,limit}(n_{e,line}) = \frac{(E_{NBI,max}-E_{NBI,min})}{(n_{e,line}(E_{NBI,max})-n_{e,line}(E_{NBI,min}))} \cdot \left(n_{e,line} - n_{e,line}(E_{NBI,max})\right) + E_{NBI,max}} \qquad (5)$$

where $E_{NBI,max}$ is 870 keV for H NBI and 1000 keV for D NBI, $E_{NBI,min}$ is 500 keV, $\boldsymbol{n_{e,line}(E_{NBI,max})}$ is the value of $n_{e,line}$ at $E_{NBI,max}$, $\boldsymbol{n_{e,line}(E_{NBI,min})}$ is $n_{e,line}$ at the $E_{NBI,min}$. Density values for eq. 5 can be read from Fig. 5a. If we now want to estimate the total available NBI power, we put eq. 5 into eq. 2 for each single injection line. Fig. 5b finally represents the total NBI power available for H and D injection in a D plasma. The NBI available power is represented versus the plasma current for different values of Greenwald density fractions ($\boldsymbol{f_{GW} = \frac{n_{e,line}}{n_{GW}}}$, where the Greenwald density is $\boldsymbol{n_{GW}[10^{20}m^{-3}] = \frac{I_p[MA]}{\pi a[m]^2}}$). Fig. 5b is produced with a density-peaking factor $n_{pf} = 1.2$.

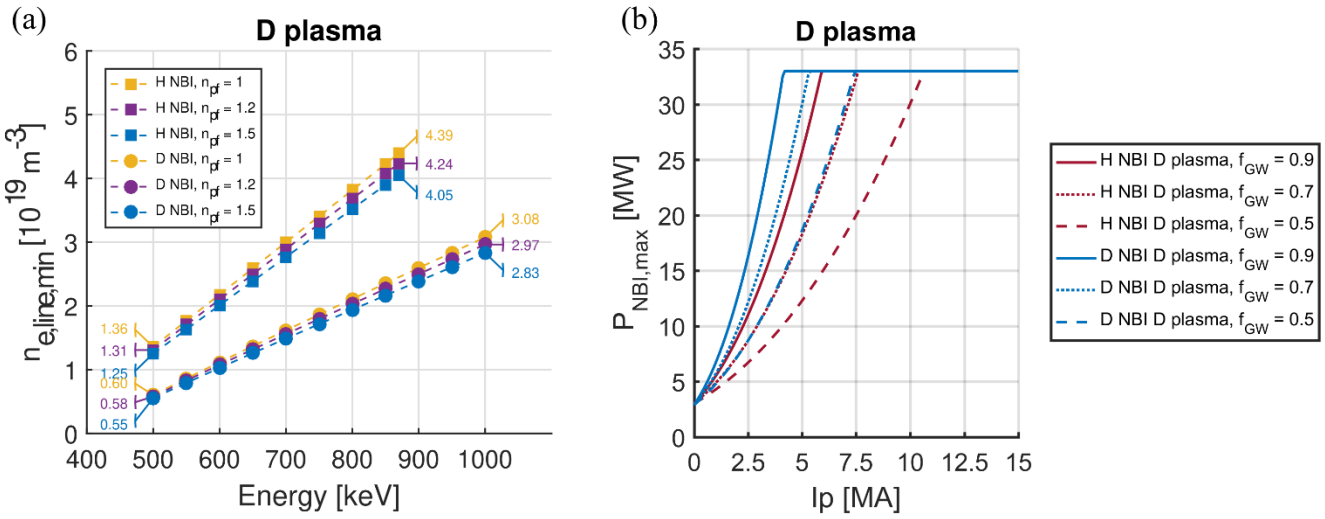

Figure 5: (a) shows the minimum line-averaged electron density $n_{e,line,min}$ for D and H NBI operations in ITER D plasmas, for different values of density-peaking factors, as a function of beam injection energy (NBI power varies as eq. 2). In (b) the H and D NBI available power in a D plasma is plotted as a function of the plasma current at different Greenwald density fractions f_{GW}.

We can now draw the operational window of ITER H and D NBI in a D plasma in a density-plasma current space in Fig. 6, assuming $n_{pf} = 1.2$. We limited the space with f_{GW} lines at $f_{Gw} = 1$ and $f_{GW} = 0.33$. The upper f_{GW} limit is a standard operational plasma density limit, which has been shown not to be a hard limit for tokamak operations (see e.g. **[28]**, **[29]**). The lower f_{GW} limit of 0.33 is for H-mode access in the high-density branch **[1]** for ITER scenarios at edge safety factor $q_{95} = 3$. We can imagine the usual ITER operations between these f_{GW} limits. The NBI operation is limited in density, as shown in Fig. 5a, depending on the beam injection energy: this further limits the NB operational window. D NBI operational window is wider than H NBI due to the lower ST (see Fig. 3b) and the lower available beam power at the same E_{NBI} with respect to H NBI due to the different $E_{NBI,max}$ value in eq. 2. The operational space widens at high current and density.

The change of the background plasma species has a smaller impact on ST than the change of the injected species. The minimum density for ITER NBI operations and the power availability results are similar for H and D-T plasmas, with a significant change only when moving from H to D NBI, similar to what is shown above for the D plasma case. Appendix A reports the minimum density to operate NBI and its maximum power for H and D-T plasma cases, similar to Fig. 5.

The operability of ITER NBIs as a function of their energy and plasma density remains the same in both steady-state and transient plasma pulse phases, provided the plasma density profile and magnetic equilibrium do not change too rapidly relative

to the beam ionisation process. With these assumptions, the NBI density limit and the power availability discussed in this section can also be applied to plasma operations during ITER transient phases such as ramp-up or ramp-down.

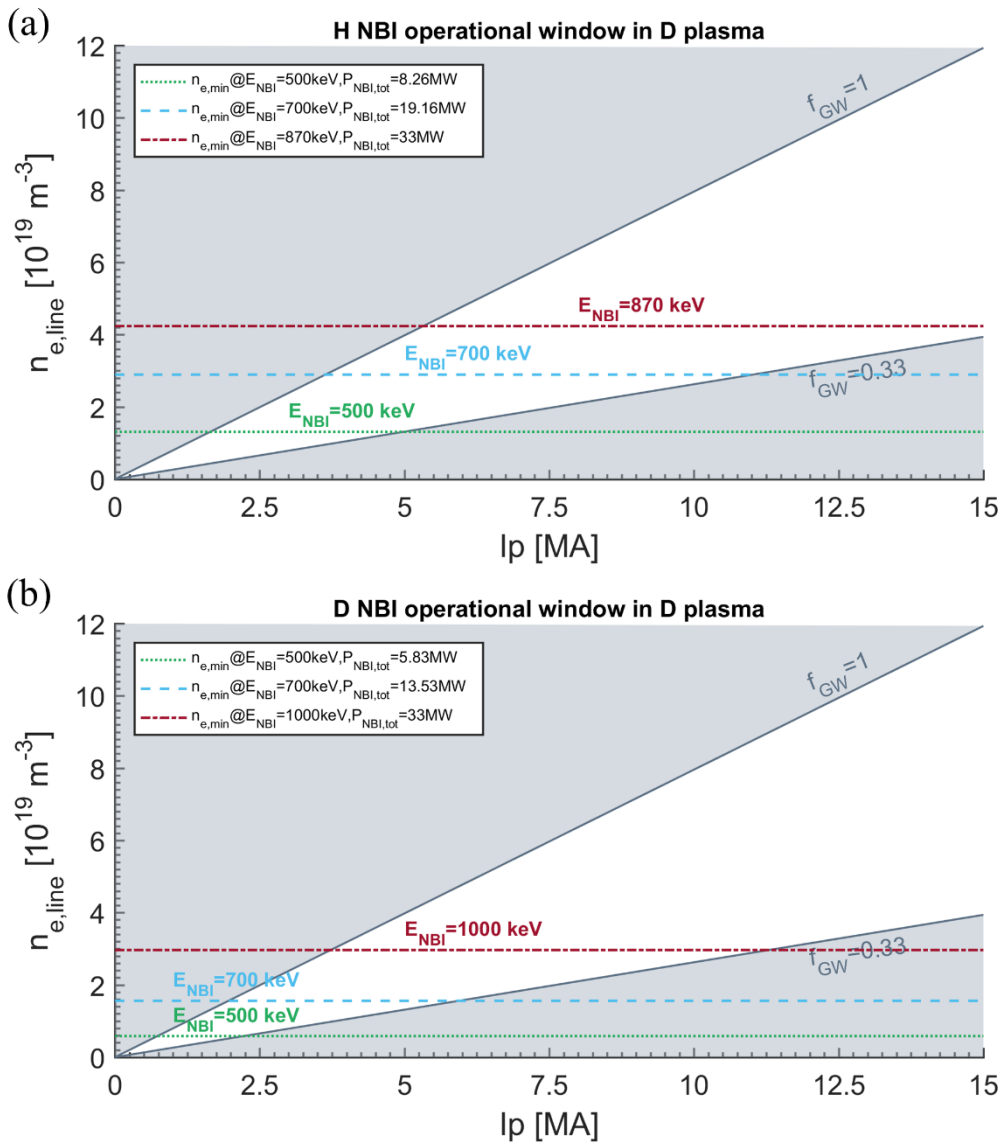

Figure 6: H and D NBI (resp. in (a) and (b)) operational window in plasma line-averaged electron density and current. Each ITER NB injector can be operated in the white region of the plots, with the minimum density depending on beam injection energy. As foreseen in ITER plasma scenarios, Greenwald density fraction limits at 0.33 and 1 are reported as approximate boundaries.

5. NBI ionisation code comparison

BBNBI and NEMO beam ionisation codes received the same input via the IMAS standard data format (Interface Data Structure, "IDS"), allowing a direct and fair comparison. Fig. 7a and 7b compare BBNBI and NEMO shine-through fractions at the same plasma density and injection energy in the range of parameters in the Tab. 1, respectively, for off- and on-axis injection geometry. For all five plasma/NBI species cases, results are in good agreement, with an overall root mean square deviation (RMSD) between BBNBI and NEMO of 0.0098 and 0.0084 for, respectively, off- and on-axis injection geometry. The deviation between the codes appears larger at high ST fractions where NEMO ST fraction prediction is larger than BBNBI, while code agreement is better in the range of interest of ITER, i.e. ST $\leq$ 0.1. The fact that BBNBI and NEMO compare similarly in the two injection geometries tends to exclude that the slight differences between the codes are due to geometrical effects in the representation of the beams within the two codes. Another difference between the codes is the use of different ionisation

cross-section models (see sec. 3). The ionisation cross-section model can explain that the deviation between the codes is more significant for D NBI than H NBI, independently of the plasma species. This fact can be seen from the figures and is quantified by an RMSE, which results 40% smaller in H NBI with respect to D NBI in the same plasma (D, D-T). BBNBI has been recently upgraded to use ADAS cross-sections **[30]**, though not yet implemented in the ITER IMAS BBNBI version.

METIS can also predict the beam ST fraction, as explained in Sec. 4. METIS has a simplified plasma equilibrium solver and describes plasma kinetic profiles on a radial grid of 21 points. When comparing METIS to the average of BBNBI and NEMO results (averaging also over the two injection lines with off- and on-axis injection geometries), we note a significant underestimate of the ST fraction for identical beam and plasma parameters, quantified in about -25% in METIS simulations. METIS has been, therefore, run with an improved plasma magnetic equilibrium calculated by the FEEQS equilibrium solver **[31]**, the MATLAB version of the NICE code **[32]**. The ST fraction results of METIS + FEEQS are compared to the average of BBNBI and NEMO in Fig. 7d. The improved magnetic equilibrium solution has a clear effect on METIS ST, with a good agreement for beam injection in H and D plasmas. Beam injection in D-T plasmas still shows a significant deviation of about ± 25%, and this discrepancy is being investigated. METIS ST deviation from BBNBI and NEMO is, therefore, due to a geometrical effect, which can be partly solved by coupling FEEQS to METIS in the case of H or D plasmas. The reason is thought to be that in METIS, the magnetic axis is assumed to be at the same vertical position as the geometric axis, which is not the case in ITER scenarios, where, e.g. at I_p = 15 MA, the magnetic axis is shifted about 25 cm upwards **[33]**. This explains why METIS underestimates the ST fraction. Looking at the beam injection geometry (Fig. 1), though with the approximated way of METIS of representing vertically shifted injection geometries, the ITER beams pass closer to the high-density plasma core if the magnetic axis is at the same vertical position of the geometrical axis. With FEEQS magnetic reconstruction that shifts the magnetic axis upwards, the beams correctly see a less-dense plasma, and the ST fraction becomes larger to values similar to BBNBI and NEMO (at least for H and D plasmas). These pieces of evidence point to a possible error when FEEQS consider D-T plasmas, as seen when looking at ST fractions in D-T plasmas (in Fig. 7d). The results here reported suggest that reactor-like plasma modelling (ITER, DEMO…) with METIS should use a more realistic plasma equilibrium to avoid significant errors in the mapping of plasma kinetic profiles in the real space.

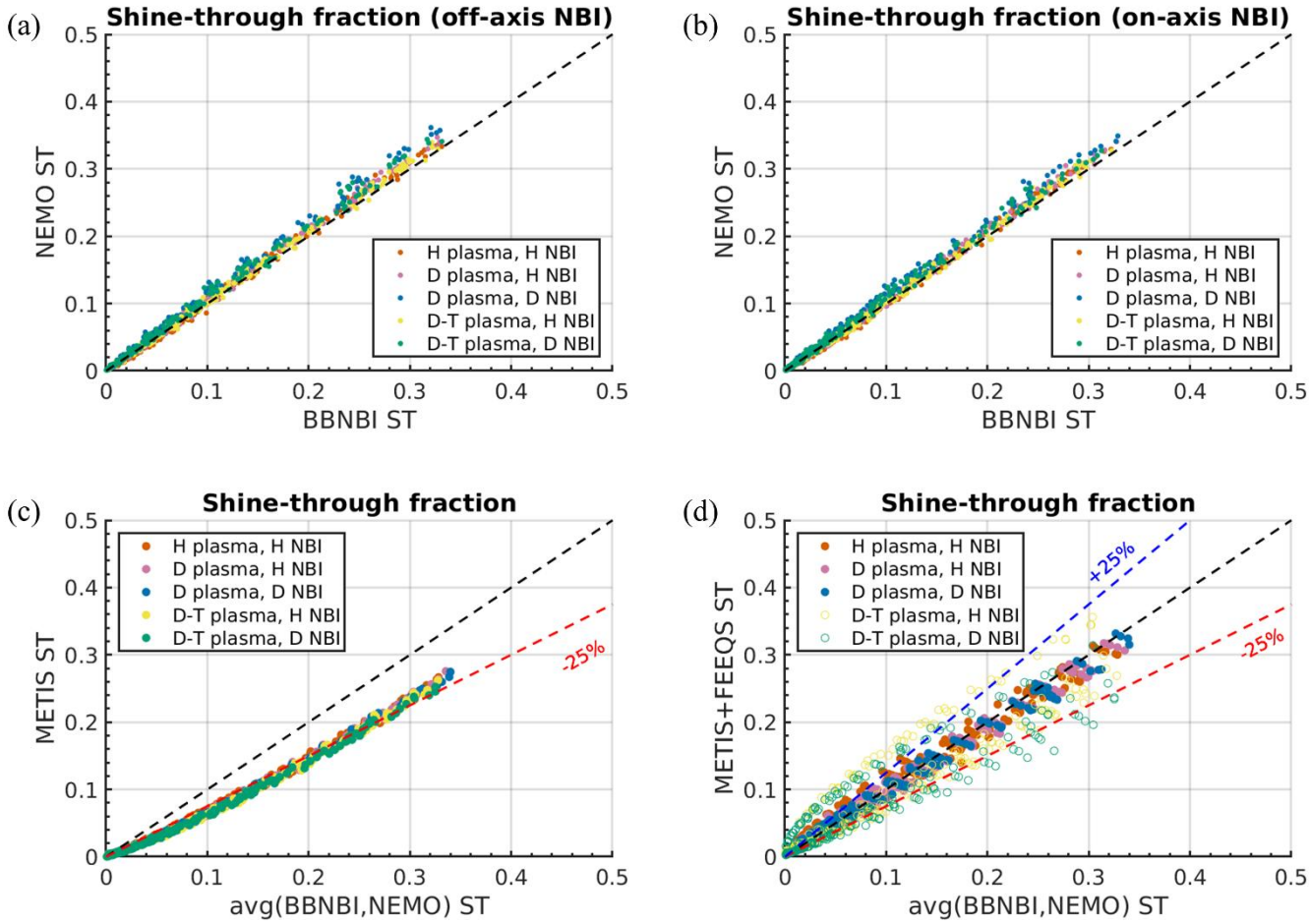

Figure 7: Ionisation code comparison. (a) and (b) report NEMO vs BBNBI shine-through fraction estimations for the parameters reported in the Tab. 1, respectively, for off- and on-axis injection configurations. In (c) METIS (and in (d) METIS coupled to FEEQS equilibrium solver), shine-through fraction prediction is compared to the average of BBNBI and NEMO codes (off-/on-axis injection geometry BBNBI and NEMO results are averaged too when compared to METIS).

6. Conclusions and future work

ITER's success relies on the effective operation of its auxiliary systems, namely the heating and current drive from radiofrequency systems and neutral beam injection (NBI). In the recently-updated ITER baseline, NBI will be available from the DT-1 phase, and it will operate in H, D and later in D-T plasmas, being a critical component to prepare and achieve $Q \geq 10$ plasmas. However, beam energetic particle losses leading to potentially harmful localised power loads must be avoided, particularly in the case of inefficient ionisation ("shine-through"). NBI operations will be only possible if shine-through losses result in power loads within the allowed plasma-facing component (PFC) limits. This paper recalculated the shine-through power load limit on the ITER PFCs through a realistic beamlet-by-beamlet projection of beam intensity on the plasma-facing components. We considered the latest blanket re-design aimed at reducing the exposition of unshielded PFC areas to the beam. This re-design allowed doubling the previous power load limit presented in **[6]**. By exploring the dependencies of shine-through losses on plasma average density, density profile shape, and injection energy through extensive numerical simulations, we have defined the operational window for NBI in DT-1 plasmas. We proposed a parametrisation of beam shine-through loss fraction and the minimum plasma density that allows NBI operation for the most promising injection geometries off- and on-axis and the various combinations of plasma/NBI species foreseen in the DT-1 phase. Shine-through losses also depend strongly on the injected species, while the change of the hydrogenic plasma species is less significant. Specifically, D NB injection results in about half shine-through losses compared to H injection, offering a wider operational range. H NBI at full energy and power can be operated above a line-averaged electron density of $4.24 \cdot 10^{19}$ m^{-3}, while $2.97 \cdot 10^{19}$ m^{-3} for D NBI in a D plasma (limits are similar in H and D-T plasmas), considering a moderately peaked density profile with a peaking factor of 1.2. A detailed comparison of the ionisation codes within the IMAS numerical framework between the BBNBI Monte Carlo code and the NEMO narrow beam model showed excellent agreement, confirming the reliability of these tools for ITER predictions. Finally,

we showed that coupling the METIS transport simulator, widely used for plasma scenario predictions, with the FEEQS equilibrium solver to improve plasma magnetic equilibrium reconstruction enhanced the accuracy of shine-through loss predictions for H and D plasmas. These findings are crucial for planning ITER's operational phases and maximising the efficiency of the NBI system while protecting the machine's integrity and ensuring the achievement of its scientific objectives. Fast and reliable tools are needed to explore wide-range parameter spaces. A new NBI modelling project has just started exploiting machine learning and artificial intelligence methods to generate Monte-Carlo surrogate tools to predict NBI ionisation, power deposition and current-drive for ITER and JT-60SA plasmas. With this project, we aim to contribute in the near future to define ITER scenarios, with the opportunity of validating our tools in the coming JT-60SA NBI operations.

Acknowledgements

This work has been done in the ITER Scientist Fellow Network framework. This work was partially funded by the Academy of Finland project No. 324759. The views and opinions expressed herein do not necessarily reflect those of the ITER Organization. The authors thank C. Bourdelle for the valuable discussions on METIS+FEEQS results.

References

[1] ITER Organization, "ITER research plan within the staged approach," ITR-18-003, 2018.

[2] P. Barabaschi, "Progress on ITER manufacturing, construction, commissioning and plans," in 29th IAEA FEC, London (UK), 2023.

[3] A. Loarte et al., "The new ITER Baseline, Research Plan and open R&D issues"," in EPS plasma conference, Salamanca (ES), submitted to Plasma Phys. Control. Fusion, 2024.

[4] A. Loarte et al., Nucl. Fusion, vol. 61, p. 076012, 2021.

[5] S. Suzuki et al., Plasma Phys. Control. Fusion, vol. 40, no. 12, pp. 2097-2111, 1998.

[6] J. Singh et al., New J. Phys., vol. 19, p. 055004, 2017.

[7] T. Kurki-Suonio et al., Plasma Phys. Control. Fusion , vol. 59, p. 014013, 2017.

[8] S. Pinches et al., Phys. Plasmas, vol. 22, p. 021807, 2015.

[9] P. Vincenzi et al., Fusion Eng. Des., vol. 200, p. 114178, 2024.

[10] R. S. Hemsworth et al., New J. Phys., p. 025005, 2017.

[11] V. Toigo et al., Fusion Eng. Des., vol. 168, p. 112622, 2021.

[12] G. Serianni et al., IEEE Transactions On Plasma Science, vol. 51, no. 3, 2023.

[13] E. Dlougach et al., Appl. Sci., vol. 12, p. 8404, 2022.

[14] E. Dlougach, "BTR Code for Neutral Beam Design," [Online]. Available: https://sites.google.com/view/btr-code/home. [Accessed 12 12 2024].

[15] ITER Organization, "Deviation Request on Plasma Heat Flux Radiation," ITER report 6XSPY5 v1.0.

[16] ITER Organization, "Preliminary thermomechanical analysis of SB 16 ST region exposed to HNB loads," ITER report B6WEPJ v1.0.

[17] F. Imbeaux et al., Nucl. Fusion, vol. 55, p. 123006, 2015.

[18] J.-F. Artaud et al., Nucl. Fusion, vol. 58, p. 105001, 2018.

[19] H. Luetjens et al., Comput. Phys. Commun., vol. 97, p. 219, 1996.

[20] M. Schneider et al., Nucl. Fusion, vol. 51, p. 063019, 2011.

[21] O. Asunta et al., Comput. Phys.Commun., vol. 188, p. 33–46, 2015.

[22] "Atomic Data and Analysis Structure (ADAS)," [Online]. Available: http://www.adas.ac.uk/. [Accessed 12 12 2024].

[23] H. Shirai et al., Nucl. Fusion, vol. 64, p. 112008, 2024.

[24] M. Cavedon, "Power losses mechanisms for neutral beam injected particles in ASDEX upgrade tokamak under different plasma configurations," Master Thesis in Physics, Università degli Studi di Padova, 2012.

[25] P. Vincenzi et al., Plasma Phys. Control. Fusion, vol. 63, p. 065014, 2021.

[26] C. De Piccoli et al., Front. Phys., vol. 12, p. 1492095, 2024.

[27] R. K. Janev et al., Nucl. Fusion, vol. 29, p. 2125, 1989.

[28] M. Giacomin et al., Phys. Rev. Lett., vol. 128, p. 185003, 2022.

[29] S. Ding et al., Nature, vol. 629, p. 555–560, 2024.

[30] L. Sanchis et al., "ASCOT simulations of helium beam-ion losses in Wendelstein 7-X," in EPS plasma conference, Salamanca (ES), 2024.

[31] H. e. al., J. Plasma Phys., vol. 81, no. 3, p. 905810301, 2015.

[32] B. Faugeras et al., Fusion Eng. Des., vol. 160, p. 112020, 2020.

[33] C. Bourdelle, Private communication, 2024.

Appendix A

We complete the information in Sec. 4 reporting the operational window of H and D NBI in ITER H and D-T plasmas. NBI limit density and available power for H NBI in H plasmas are reported in Fig. 8.

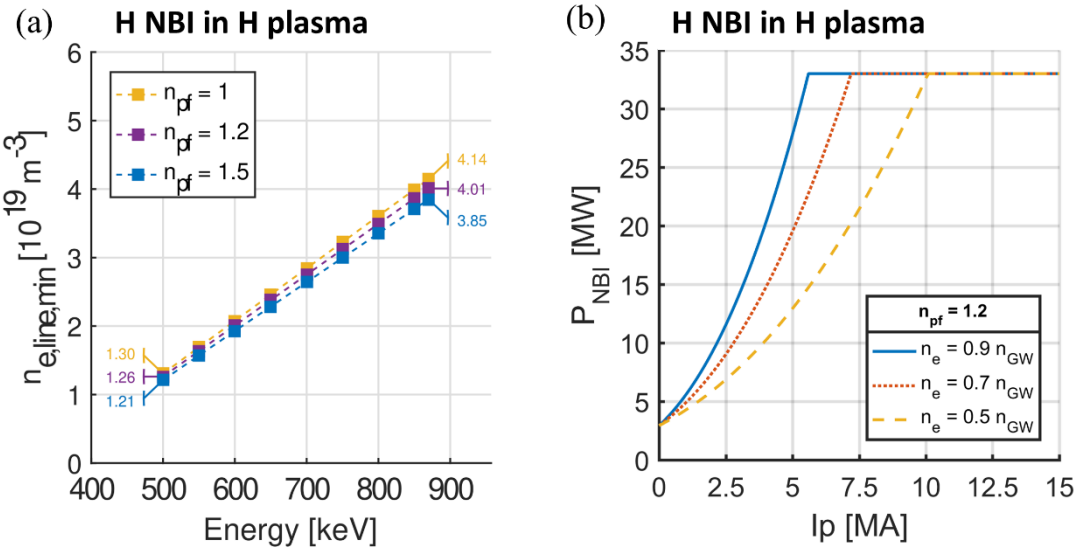

Figure 8: (a) shows the minimum line-averaged electron density $n_{e,line,min}$ for H NBI operation in ITER H plasmas, for different values of density-peaking factors, as a function of beam injection energy (NBI power varies as eq. 2). In (b) the H NBI available power in a H plasma is plotted as a function of the plasma current at difference Greenwald density fractions f_{GW}.

The minimum density to operate NBI in D-T plasmas and the available power at different plasma currents are reported in Fig. 9.

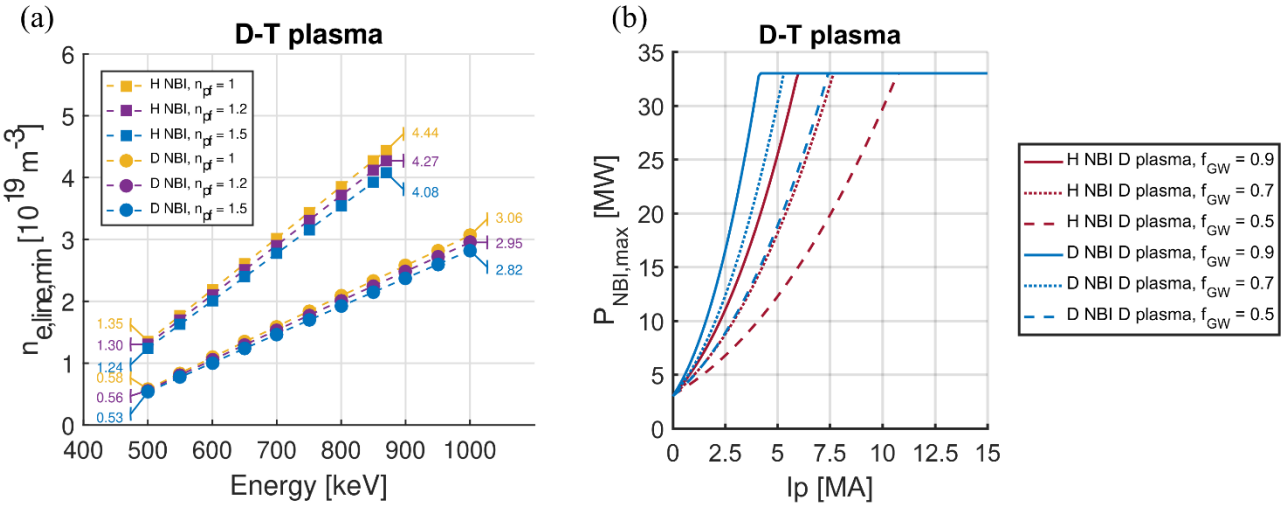

Figure 9: (a) shows the minimum line-averaged electron density $n_{e,line,min}$ for H and D NBI operations in ITER D-T plasmas, for different values of density-peaking factors, as a function of beam injection energy (NBI power varies as eq. 2). In (b) the H and D NBI available power in a D-T plasma is plotted as a function of the plasma current at difference Greenwald density fractions f_{GW}.

Last, the operational space in plasma current and density of H and D NBI in H and D-T plasmas is reported in Fig. 10 for different injection energies.

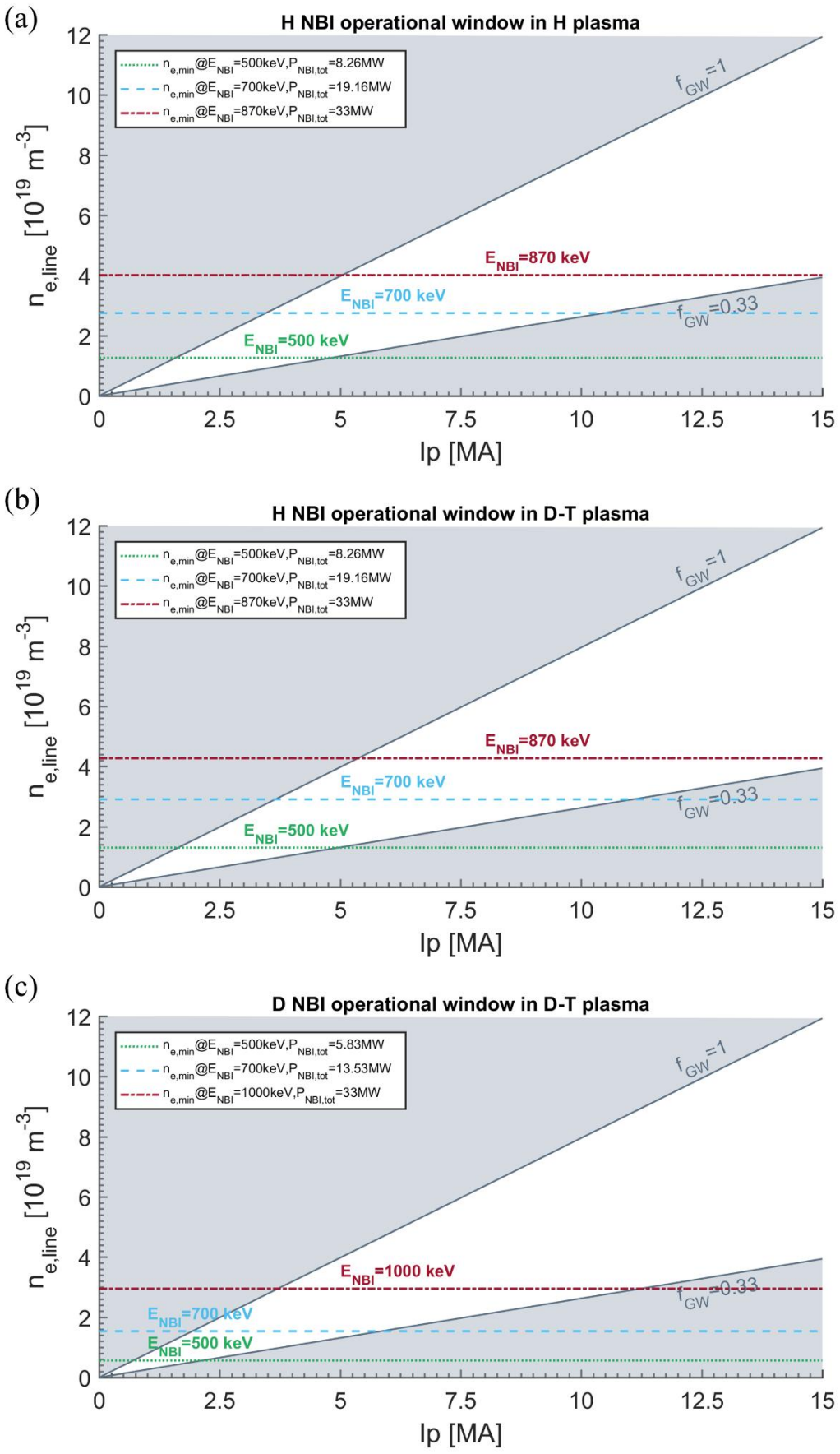
(a)
H NBI operational window in H plasma
$n_{e,min}$@E_{NBI}=500keV,$P_{NBI,tot}$=8.26MW
$n_{e,min}$@E_{NBI}=700keV,$P_{NBI,tot}$=19.16MW
$n_{e,min}$@E_{NBI}=870keV,$P_{NBI,tot}$=33MW
f_{GW}=1
E_{NBI}=870 keV
E_{NBI}=700 keV
f_{GW}=0.33
E_{NBI}=500 keV
$n_{e,line}$ [10^{19} m^{-3}]
Ip [MA]
(b)
H NBI operational window in D-T plasma
$n_{e,min}$@E_{NBI}=500keV,$P_{NBI,tot}$=8.26MW
$n_{e,min}$@E_{NBI}=700keV,$P_{NBI,tot}$=19.16MW
$n_{e,min}$@E_{NBI}=870keV,$P_{NBI,tot}$=33MW
f_{GW}=1
E_{NBI}=870 keV
E_{NBI}=700 keV
f_{GW}=0.33
E_{NBI}=500 keV
$n_{e,line}$ [10^{19} m^{-3}]
Ip [MA]
(c)
D NBI operational window in D-T plasma
$n_{e,min}$@E_{NBI}=500keV,$P_{NBI,tot}$=5.83MW
$n_{e,min}$@E_{NBI}=700keV,$P_{NBI,tot}$=13.53MW
$n_{e,min}$@E_{NBI}=1000keV,$P_{NBI,tot}$=33MW
f_{GW}=1
E_{NBI}=1000 keV
f_{GW}=0.33
E_{NBI}=700 keV
E_{NBI}=500 keV
$n_{e,line}$ [10^{19} m^{-3}]
Ip [MA]

Figure 10: Operational windows of H NBI in H plasma (a), H (b) and D (c) NBI in D-T plasmas in the plasma density-current space.